COMPUTER SIMULATION OF ESD FROM VOLUMINOUS OBJECTS COMPARED TO TRANSIENT FIELDS OF HUMANS

R. Jobava, *Member, IEEE,* D. Pommerenke, *Member, IEEE,* D. Karkashadze, *Member, IEEE,* P. Shubitidze, *Student Member, IEEE,* R. Zaridze, *Member, IEEE,* S. Frei, M. Aidam (now TU Muenchen)

Hewlett Packard, Roseville CA
Tbilisi State University
Technical University Berlin

***Abstract* – Computer simulation of ESD for simplified objects is described and compared to measured transient fields of human/metal ESD. The simulation algorithm uses the Method of Moments in time domain, coupled with non-linear arc resistance model. Transient currents and fields are analyzed from EMC point of view. Validation of the numerical simulation is done by comparison to experimental data. The simulated structure models the human/metal ESD in its peak current and field values and their derivatives reasonably well.**

Keywords
Indirect ESD, transient fields, Method of Moments, arc resistance

I. INTRODUCTION

Electrostatic discharge (ESD) is a well-recognized threat to electronics. Of all impulsive disturbances, it has the shortest risetime with a lower risetime limit about 20 ps for voltages above 1.5 kV [1]. The discharge is associated with strong fields, for example, a 0.7 ns risetime human/metal discharge at 5 kV will cause a magnetic field of approx. 30 A/m and an electric field of 12 kV/m at 0.1 m distance (arc length 0.8 mm) [2]. Such large fields can easily disturb electronic systems. They may even permanently lose functionality e.g. by latch-up, by the loss of information stored in flash memory or by hardware damage, which is often seen in MR-heads [3].

Considerable effort has been devoted into the study of ESD current waveforms [1,4,5,6,7,8,9,10]. Of particular interest are the amplitude and rise-time variations due to different voltages, approach speeds and electrode shapes. In contrast to most high voltage breakdowns, air discharge ESD occurs mostly between approaching objects. The low reproducibility of air discharge ESD is well known e.g. with the same object and charge voltage discharge currents and fields vary by large amounts. Different reasons such as corona have been offered to explain this phenomena [7,8,11]. But real reason behind the low reproducibility is the combined influence of statistical time lag (see appendix) and speed of approach [1,9,12] that allows the gap to close further. Most ESD occur at gap distances smaller than the Paschen value (see appendix). The electrostatic field increases as the gap closes. The increased field enhances the ionization processes once the discharge is initiated. The shorter the gap is for a given voltage, the faster the discharge current will rise. Measurements show [1] that the peak current derivative may vary by up to three orders of magnitude for discharges with the same object, at the same voltage just due to different arc lengths (see appendix).

In Fig.1 measured peak current derivatives are shown as a function of arc length for hand/metal ESD into a broadband current sensor [13]. Measurements were taken at different approach speeds and humidities. The measurement bandwidth was approx. 3 Ghz (SCD 5000 with compensated external delay line). The peak current derivative increases from 3 A/ns to 600 A/ns with reduced arc length. Such a change has severe consequences on the severity as an EMC threat making it necessary to characterize electrostatic air discharges not only by the object and voltage but additionally by their arc lengths. Furthermore, the strong dependence on the arc length provides important criteria for testing the usability of electromagnetic and arc models.

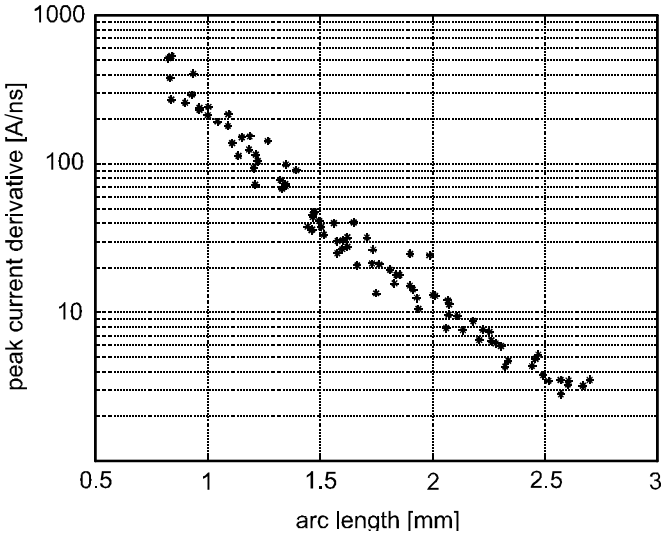

Fig.1. Measured peak current derivatives versus arc length for hand/metal ESD using a small metal rod (6 cm long, 8 mm diameter) at 10 kV. All measurements shown in this article were done at about 60 m above sea level. The object's voltage was kept constant by connecting it via a Mega-ohm resistive wire to a power supply.

Calibrated transient field measurements of ESD are rare [1, 9,14, 15,16,17]. Some analytical estimations and numerical calculations of transient fields of ESD have been published [14,15,18,19,20,21,22,23]. Wilson and Ma [14] modeled the radiating elements as an electrically small dipole excited by measured discharge current. In their measurements, they only used static breakdown, i.e. ESD having arc lengths in accordance to the Paschen law. This lead to very slow rising ESD waveforms. They assumed that the arc and some part of the discharging structure cause the radiation. This has often been misinterpreted as if only the arc radiates. But as pointed out in [24] not only the arc but the complete structure radiates. A small dipole model may fail to predict important characteristics [23]. Ishigami used a cosine distribution and measured discharge currents. Fujiwara [18] used the small dipole model and obtained the currents by analytically solving the discharge of two point charges via an arc. Later he simulated sphere discharges using FDTD but obtained the current from measurement [23]. To model the arc he used Rompe and Weizel's law [25] and arc lengths as given by the Paschen law calculated the current ahead of the FDTD calculation. Angeli [19] used FDTD to model the discharging object but did take the arc into acount. Coupling into enclosures was calculated via FDTD by Angeli and Van den Berghe [20,26] using current waveform given by the IEC standard and by Cerri using measured currents [27]. But the reported calculations are incomplete, as they do not couple the arc to the discharging structure. Without an arc model, the field from ESD can only be calculated if measured currents are used or if the currents are obtained by other means like analytical estimations.

The objective of this work was to develop an efficient algorithm for computer simulation of ESD, which includes both the object and the arc. Due to the non-linearity of the arc, the time-domain methods are preferable.

But the dimensions are hard to handle numerically. One needs to know the electric field in the arc very accurately. But the arc is less than 3 mm long, very small compared to the object size of up to 1 m. In a first step, a simple thin wire algorithm had been developed to simulate a discharging rod [1, 9]. In this paper, results are presented for perfectly conducting bodies of revolution discharging through an arc into an infinite large ground plane at a given initial voltage and arc length.

The proposed algorithm is based on the Method of Moments (MoM) in the time domain and models the non-linear arc. Its linear part has been validated against literature data. The complete algorithm has been validated against measured data. Additionally, it is shown that a simplified

geometry can be used to approximate peak current, fields and their derivatives for human/metal ESD.

II. PROBLEM SOLVED

We simulate the discharge of a perfectly conducting body of revolution which approaches a ground plane being charged to a fixed voltage as shown in Fig. 2.

At some distance *h* from the plane the breakdown occurs. If the electrostatic field is quasi homogeneous (no pre-breakdown space charges) and the statistical time lag negligible, Paschen's law will predict the distance *h*. But for most practical cases, the statistical time lag can not be neglected, i.e. *h* will be smaller than the value predicted by Paschen's law.

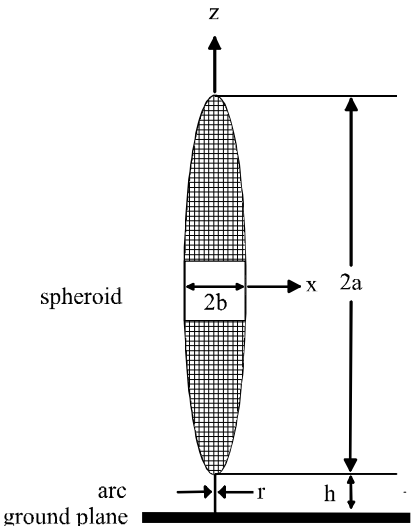

Fig. 2. Geometry of the problem. A and b: semiaxis of the spheroid, h: arc length, r: arc diamter. The z-axis is the axis of revolution.

For realistic approach speeds, the electric field prior to breakdown can be treated as an electrostatic field. Initial condition of the dynamic breakdown process is the electrostatic charge distribution on the surface.

The algorithm consists of the two subparts: electrostatic and dynamic.

1. Electrostatic

   First the electrostatic problem is solved. The resulting electrostatic charge distribution can be considered as initial data for the transient process.

2. Dynamic

   Ohm's equation in its differential form is used to describe the transient non-linear process in the arc. To obtain the conductivity we use the model of Rompe and Weizel.

   The redistribution of charges on the discharging body and its mirror image are derived from a time domain formulation of the magnetic integral equations. MoM solves this boundary value problem directly in the time domain.

   The arc current influences the charge distribution on the body in two ways: by fields radiated from the arc, and by current flowing from the arc onto the surface, which does Kirchhoff's law models.

III. ELECTROSTATIC CONSIDERATION

Once the charging process has come to an end, the voltage is determined by the capacitance, by corona losses or by charge drainage through high impedance ground paths. Neglecting charge losses, only the capacitance will determine the voltage. It changes during the approach to ground.

Fig.3 presents the calculated capacitance of the spheroid as a function of the distance to the ground plane as calculated by a simplified algorithm based on the Method of Auxiliary Sources [28,29]. The spheroid's free space capacitance value is 13.549 pF.

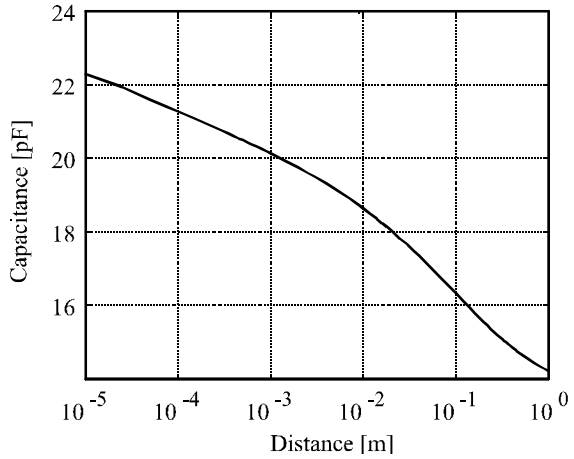

Fig.3: Calculated capacitance to ground for a spheroid of a= 31 cm and b = 5 cm semi-axis. See fig. 2 for the geometry.

Assuming an initial voltage of 10 kV at a distance of 1 m the voltage will drop to 7.2 kV at a distance of 1.8 mm. Consequences are:

1) Even if a further reduction of the gap length due to the combined influence of the statistical time lag and speed of approach does not take place, the reduced voltage will cause a faster rising discharge current as breakdown field strength in air increases as the voltage goes down.
2) The enhanced charge accumulation at the ground plane and the lower tip will cause a higher peak current value.
3) A voltage value measured in a position other than the discharge position will not represent the voltage at the beginning of the sparking.

The charge density distribution along the generating line of a spheroid (semi-axis 31 cm - 5 cm, voltage: 5 kV, gap-length: 0.6 mm) is shown in fig.4. A large portion of the charge is concentrated near the channel. The steep electric field gradients near the gap require very accurate calculations in this area.

The breakdown process is greatly affected by the amount of charge in the lowest part of the body. For rotational bodies with a smooth lower tip the more charge is concentrated close to the gap, the larger the peak current will be.

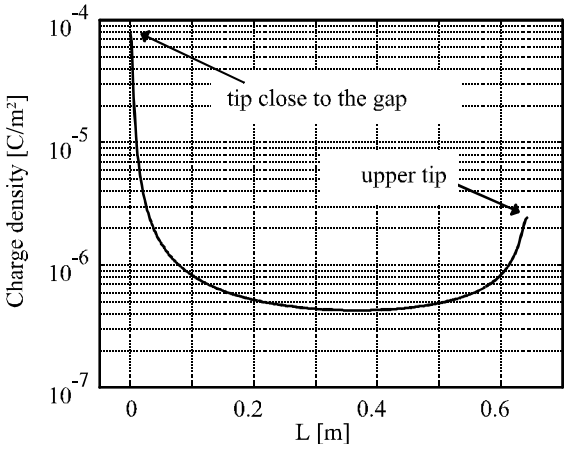

Fig. 4: Charge density along the generating line of the spheroid.

Fig. 5 shows normalized experimental current maximas compared to normalized calculated maximas of electrostatic charge densities. The values were obtained the following way: For each voltage peak currents were measured at different arc lengths using 3 GHz bandwidth [1,2]. Those peak currents were normalized to the largest peak current measured at that voltage and plotted. Charge density calculations were done at the same arc lengths and voltages as in the experiment. They again were normalized to the largest charge density value for each voltage level and plotted. From these figures it can be seen, that I_{max} is proportional to the charge density at the lower tip of the spheroid. The coefficient of proportionality depends on the voltage V. Most likely this holds true for convex bodies, but we may not generalize the proportionality between peak charge density and peak current as it has not been tested sufficiently for other geometry.

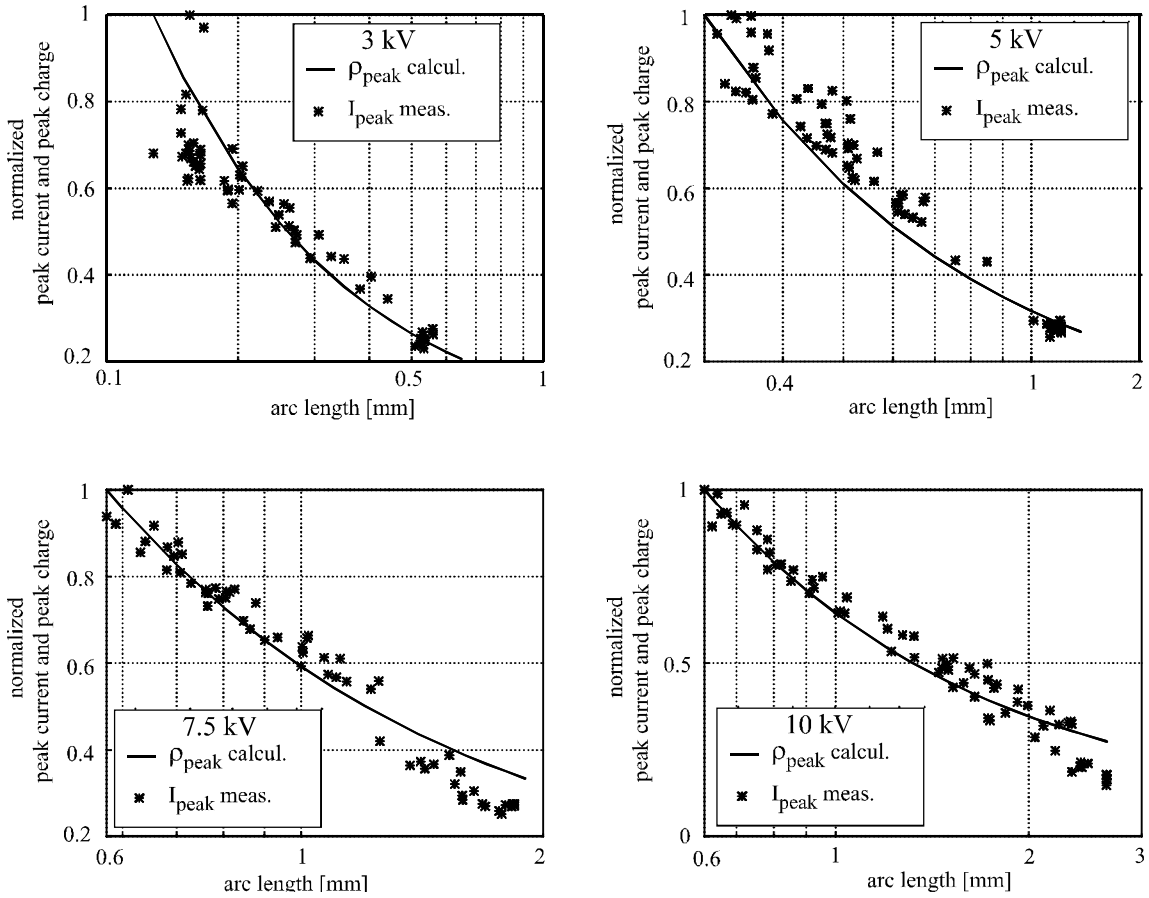

Fig.5. Relative relationship between peak discharge current and maximal charge density prior to the discharge for different voltages as a function of arc length.

IV ARC MODEL FOR ESD

The arc is electrically small; i.e. a time dependent resistor can model it. A choice of empirical models and models which take basic ionization processes into account exist. Examples are the models by Braginski [30], Rompe and Weizel [31], Toepler [25], Mesyats [32,33] and others [34,35,36,37,38,39].

For current values and time frames typical for ESD the models of Rompe and Weizel [31] and Mesyats [32] are preferable as they reproduce the influence of the arc length on the discharge current correctly [1,9]. Only for arc lengths in accordance to the Paschen law, Toepler's law provides results similar to Rompe and Weizel's equation leading to the wrong impression [5] that ESD can be modeled using Toeplers law. But Toeplers law cannot reproduce the influence of the arc length on the discharge current correctly [1, 9].

According to the model of Rompe and Weizel the arc resistance as a function of time is given by:

$$R(t) = \frac{2h}{\sqrt{2a_R \int_0^t I_{arc}^2(t')dt'}} \qquad (1)$$

Where R(t) is arc resistance ([Ohm]), 2h is length of arc and its image ([m]), $I_{arc}(t)$ is arc current ([A]), a_R a parameter ([m^2/V^2sec]) derived from basic ionization processes [31,34], t is time ([sec]). Expression (1) implies a constant electrical field along the channel.

In the numerical implementation an initial resistance value of 1 MOhm or 10 MOhm was used to start the discharge process. As long as the initial resistance value is much larger than the arc resistance during the important phase of the discharge, any value can be chosen. The discharge wave shape will not be influenced; it will only be shifted in time.

Ideally, a_R would be a constant. Due to the numerous simplifications in Rompe and Weizel's law, some deviations between the real arc resistance and the calculated one must be expected. Literature values for a_R in air under normal pressure mostly derived using only slightly overvoltaged spark gaps are in the range of 0.5 10^{-4} to 2 10^{-4} m^2/V^2sec [33,32,34,36, 40]. If a_R is assumed to be independent of voltage and arc length a general match between simulated and measured ESD results [9] is achieved at a value of 1 10^{-4} m^2/V^2sec. But some differences remain. The simulation provides somewhat too short rise-times at long arc lengths and too long rise-times for short arc lengths. The deviations are not very severe judged against the overall influence of the arc length: Although the peak current derivative changes more than two orders of magnitude with arc length (fig. 1), the predicted derivative does not deviate more than 50% from the measured values [9]. To analyze which simplifications cause this deviations is beyond the scope of this paper but the simulation can be improved by modifying the value for a_R.

While investigating highly overvoltaged spark gaps for impulse shaping, Mesyats [33, 32, 40] realized that calculations using Rompe and Weizel's law will not provide fast enough current rises if values as mentioned above are used. To overcome this, one can adjust a_R to larger values for strongly overvoltaged ESD events. But the values need to be derived by an experiment, which is independent of the measurements or simulations to which we are applying the improved a_R values.

To do so, a 150 Ohm TEM line was discharged while measuring current and arc length [9]. The currents were compared to a SPICE simulation using Rompe and Weizel's law. This lead to the values of Table 1 which are more suitable for ESD than a constant value for a_R. But one must be aware of the limitations of air discharge models: At voltages below 1000 V or at strongly overvoltaged spark gaps at higher voltages surface processes start to dominate the ionization, somewhat similar to a vacuum breakdown. It is questionable to apply air discharge physics to the Charged Device Model simulations as it has been done in [12,41].

Table 1: Range of a_R values for ESD calculation

Voltage [kV]	**Arc length [mm]**	a_R **[m²/V²sec]**
3.0	0.57 Paschen value	0.5 to $1.0 \cdot 10^{-4}$
	0.4	1.0 to $2.0 \cdot 10^{-4}$
	0.3	1.5 to $2.5 \cdot 10^{-4}$
5.0	1.1 Paschen value	0.5 to $1.0 \cdot 10^{-4}$
	0.9	0.8 to $1.2 \cdot 10^{-4}$
	0.5	1.0 to $3.0 \cdot 10^{-4}$
7.5	1.9 Paschen value	0.5 to $1.0 \cdot 10^{-4}$
	1	1.0 to $2.0 \cdot 10^{-4}$
	0.5	2.0 to $3.0 \cdot 10^{-4}$
10.0	2.7 Paschen value	0.5 to $1 \cdot 10^{-4}$
	2	0.8 to $1.5 \cdot 10^{-4}$
	1	2.0 to $3.5 \cdot 10^{-4}$
	0.7	2.0 to $4 \cdot 10^{-4}$

Presently we could not narrow the ranges given any further. This is caused by the uncertainty in the arc length measurement (+/- 30 μm), the estimation of the stray capacitance between the TEM line and the current sensor and due to the bandwidth limit of the oscilloscope (SCD5000 with frequency compensated external delay line, approx. 3.5 Ghz bandwidth see).

All a_R values used for simulations were within the range given in Table 1.

V. THE TRANSIENT PROCESS ON THE BODY

This section describes the dynamic process. The object is considered as an antenna excited by the discharge current. As the excitation is non-linear, the numerical analysis of the transient fields is preferably done in time domain. This allows the combination of the antenna algorithm [42,43,44,45,46] with a physical description of the ionization process in the arc [1, 9, 49].

Let us consider this model in detail. In the moment before the discharge, the static charge distribution $\rho_{stat}(\vec{r})$ is known on all metallic surfaces. During the discharge, this distribution will be disturbed. Let us denote this charge disturbance by $\rho_{trans}(\vec{r},t)$. The total charge density in any point on the surface of the body or on the plane is $\rho(\vec{r},t) = \rho_{stat}(\vec{r}) + \rho_{trans}(\vec{r},t)$. The surface current density $\vec{J}(\vec{r},t)$ relates to the transient part of the charge density. So the transient problem is to find the surface current densities $\vec{J}(\vec{r},t)$ and the arc-current density $\vec{J}_{arc}(\vec{r},t)$. Using these quantities all charges and fields can be calculated. The mathematical model for $\vec{J}(\vec{r},t)$ and $\vec{J}_{arc}(\vec{r},t)$ is formulated as follows.

1. On perfectly conducting surfaces $\vec{J}(\vec{r},t)$ satisfies the Integral Equation for the Magnetic Field (IEMF):

$$\vec{J}(\vec{r},t) = 2\hat{n} \times \vec{H}^{arc}(\vec{r},t) + \frac{1}{2\pi}\hat{n} \times \int_S \left\{ \frac{\vec{J}(\vec{r}',\tau)}{R} + \frac{1}{c}\frac{\partial}{\partial\tau}\vec{J}(\vec{r}',\tau) \right\} \times \frac{\vec{R}}{R^2} ds, \qquad (2)$$

where $\vec{r}$ is located on the metallic surface S.

2. In each point of the arc the current density satisfies Ohm's differential law:

$$\vec{J}_{arc}(\vec{r},t)=\sigma(\vec{r},t)\cdot\left(\vec{E}_{stat}(\vec{r})+\vec{E}^{arc}_{trans}(\vec{r},t)+\vec{E}^{surf}_{trans}(\vec{r},t)\right), \quad (3)$$

where $\vec{r}$ is located in the volume of arc.

3. Initial values are written as follows:

$$\begin{cases}\vec{J}(\vec{r},t)=0;\\ \vec{J}_{arc}(\vec{r},t)=0;\\ \quad_{trans}(\vec{r},t)=0.\end{cases} \quad (4)$$

Let us consider some terms of these expressions. In equation (2) $\vec{H}^{arc}(\vec{r},t)$ is the magnetic field on the metallic surface caused by fields radiated by the arc-current. It is given by:

$$\vec{H}^{arc}(\vec{r},t)=\frac{1}{2\pi}\int_{V_{arc}}\left\{\frac{\vec{J}_{arc}(\vec{r}',\tau)}{R}+\frac{1}{c}\frac{\partial}{\partial\tau}\vec{J}_{arc}(\vec{r}',\tau)\right\}\times\frac{\vec{R}}{R^2}dv_{arc} \quad (5)$$

Here V_{arc} is the volume of the arc and its mirror image. S is the area of the surface of the body and of its image. $\vec{r}$ is the point of observation, $\vec{r}'$ is the point of integration, τ is the delay time: $\tau=t-\frac{R}{c}$; $R=|\vec{R}|$, and $\vec{R}=\vec{r}-\vec{r}'$. c is the speed of light, $\hat{n}$ is the outer normal of the surface. In equation (3) $\vec{E}_{stat}(\vec{r})$ is the electrostatic field of the charge distribution before the discharge. This field initiates the spark. $\vec{E}^{arc}_{trans}(\vec{r},t)$ are the transient fields radiated by the arc and its mirror image and $\vec{E}^{surf}_{trans}(\vec{r},t)$ is the transient field radiated by the body and its mirror image. These fields are calculated by:

$$\vec{E}^{arc}_{trans}(\vec{r},t)=\frac{1}{4\pi}\int_{V_{arc}}\left\{\mu\frac{1}{R}\frac{\partial\vec{J}_{arc}(\vec{r}',\tau)}{\partial\tau}-\left[\frac{\rho_{arc}(\vec{r}',\tau)}{R}+\frac{1}{c}\frac{\partial}{\partial\tau}\rho_{arc}(\vec{r}',\tau)\right]\frac{\vec{R}}{\varepsilon R^2}\right\}dv_{arc}, \quad (6.a)$$

$$\vec{E}^{surf}_{trans}(\vec{r},t)=\frac{1}{4\pi}\int_{S}\left\{\mu\frac{1}{R}\frac{\partial\vec{J}(\vec{r}',\tau)}{\partial\tau}-\left[\frac{\rho(\vec{r}',\tau)}{R}+\frac{1}{c}\frac{\partial}{\partial\tau}\rho(\vec{r}',\tau)\right]\frac{\vec{R}}{\varepsilon R^2}\right\}dS, \quad (6.b)$$

Let us consider only bodies of revolution. We introduce the system of orthogonal surface coordinates with the unit vectors: $\vec{n}_u=\frac{\vec{r}_u}{|\vec{r}_u|}$, $\vec{n}_v=\frac{\vec{r}_v}{|\vec{r}_v|}$, where u is "radial" coordinate or the coordinate along the generating line, and v is the "azimuth" coordinate, $\vec{r}_u=\partial\vec{r}/\partial u$, $\vec{r}_v=\partial\vec{r}/\partial v$, $\vec{r}_u\cdot\vec{r}_v=0$. For bodies of revolution only radial currents exist. The IEMF can be rewritten as:

$$J_u(\vec{r},t)=-2H^{arc}{}_v(\vec{r},t)-\frac{1}{2\pi}\int_{S}\left(\frac{J_u(\vec{r}',\tau)}{R}-\frac{1}{c}\frac{\partial J_u(\vec{r}',\tau)}{\partial\tau}\right)G(\vec{r},\vec{r}')dS, \quad (7)$$

with $G(\vec{r},\vec{r}')=\frac{\vec{R}[\vec{n}_u\times\vec{n}_v]}{R^2}$.

The MoM solves this equation. Let us consider some computational problems arising during the numerical realization of the MoM algorithm.

At first a space and time segmentation is done. The simplest scheme for discretisation is uniform discretisation $(\Delta l \times \Delta l \times \Delta t,$ where $\Delta l = c\Delta t.)$. Since integration is performed in the space coordinates, subsectional collocation with a δ-pulse approximation in space can be used. Using Galerkin's method we can write a discrete analogue of equation (7):

$$J_u(i,j) = \frac{1}{1-\beta_i}(-2H_v^{arc}(i,j) - \frac{1}{2\pi}\sum_{k=1}^{N_s}\oint_{\Delta S_k}\left\{\frac{J_u(k,\tau)}{R} + \frac{1}{c}\frac{\partial J_u(k,\tau)}{\partial \tau}\right\}G_{vu}^{k,i}ds) \quad (8)$$

Here *i* is used to number the belts (we assume that the body is divided into N_s belts), *j* is used for time steps, ΔS_k is the area of *k*-th belt. In addition, each belt is subdivided into M_k patches. M_k depends on the number of belt *k*. For all patches except in the case of i=k and for the patch nearest to the arc, the integral in (8) is approximated as follows: The current density is assumed to be constant on the patch. Instead of integrating we multiply the Green's function with ds, the area of the patch. The Green function is calculated for the center of the patch. For the first patch we assume that the current is constant, but not the current density.

Integration is done by Gauss law. This special treatment for the first patch is needed as it is very close to the arc. When *k=i* the small area around the point of observation contains the current $J_u(i,j)$. The effect of this area on the right side of the integral (8) can be expressed by the self-influencing integral. To underline this fact we use the notation $\oint$. The portion of the field radiated by the self-patch can be taken into account assuming that the current density is constant along the patch:

$$\int_{selfpatch} \ldots = \beta J,\ \beta = \frac{1}{2}\sqrt{\frac{\Delta S_0}{4\pi}}(k_u - k_v), \quad (9)$$

where k_u and k_v are the principle curvatures of the surface and ΔS_0 is the area of small patch [29].

For a spheroid with semi-axis a and b we have:

$$G_{vu}^{k,i} = \frac{(x-x')T_z - (z-z')T_x}{R^2} \quad (10)$$

$$T_x = \frac{b\cdot\cos(u')\cos(v')}{\sqrt{(b\cdot\cos(u'))^2 + (a\cdot\sin(u'))^2}}$$

$$T_z = -\frac{a\cdot\sin(u')}{\sqrt{(b\cdot\cos(u'))^2 + (a\cdot\sin(u'))^2}} \quad (11)$$

$$R = \sqrt{(x-x')^2 + y'^2 + (z-z')^2}$$

$$0 \le u \le \pi, \quad 0 \le v \le \frac{\pi}{2}.$$

$$x = b\cdot\sin(u) \qquad x' = b\cdot\sin(u')\cos(v')$$

$$y = 0 \qquad y' = b\cdot\sin(u')\sin(v')$$

$$z = a\cdot\cos(u) \qquad z' = a\cdot\cos(u')$$

It should be noted that actually $G_{vu}^{k,i}$ should be rewritten because it also contains the mirror image of the body.

For the calculation of the retarded time, it is necessary to know the time delay between the event, which caused the field and the reaction at the point of observation. This is given by $\tau = t - R/c,\ R/c = (n+\gamma)dt,$ where n is an integer, and $0 \le \gamma \le 1.$ A two-point smoothing approximation was used for the current and its derivative:

$$J(u',\tau) = (1-\gamma)J(u',(j-n)dt) + \gamma J(u',(j-n-1)dt). \quad (12)$$

Due to the chosen time/space discretisation, coupling between neighboring patches is always delayed by at least one time step. This allows calculating the inter-patch coupling by previously calculated current densities. The obtained current distribution is used to calculate the transient fields.

The most critical part of the algorithm is the coupling of the arc to the patch nearest to the arc. The fields in the arc contain only a z-component. Static calculation show that $E_{stat}(\vec{r})$ differs along short arc (0.1-1 mm) by less than 7 %. We assume that the current along the channel is constant. Now we integrate equation (3) over the channel and its image. We obtain:

$$R(t)I_{arc}(t) = \int_{-h}^{h} E_{stat}(z)dz + \int_{-h}^{h} E_{trans}^{arc}(z,t)dz + \int_{-h}^{h} E_{trans}^{surf}(z,t)dz, \quad (13)$$

where $R = \dfrac{2h}{S_0\sigma(t)}$ and S_0 is the area of cross section of the spark channel.

E_{stat} can be calculated accurately using electrostatic methods. If the current is constant along the channel ρ_{arc} and $\partial\rho_{arc}/\partial\tau$ are equal to zero in the arc.

Assuming that we observe the arc current at the plane z=0 we can re-write the second term (13) as:

$$\int_{-h}^{h} E_{trans}^{arc}(z,t)dz = 2h \cdot E_{trans}^{arc}(z=0,t) = -L\frac{dI_{arc}}{dt}, \quad (14)$$

where $L = \dfrac{2h\cdot\mu}{4\pi}\int_{-h}^{+h}\dfrac{dz}{R}$.

Since the point of observation is near the surface, we can express $E_{trans}^{surf}(t)$ in the channel as normal component of electric field at lower tip of the discharging body:

$$E_{trans}^{surf}(z,t) = \frac{\rho_{trans}^{(1)}(t-(h-z)/c)}{\varepsilon_0} \quad (15)$$

$(h-z)/c$ denotes the time-delay between the transient charge and its effect on the body. We also assume a permittivity of ε_0 within the arc. By $\rho_{trans}^{(1)}(t)$ we denote the charge density in the lowest part of the object. Easily we can find the charge $q_{trans}^{(1)}(t)$ on the belt close to the arc.

$$\frac{dq_{trans}^{(1)}}{dt} = I_1(t) - I_{arc}(t) \quad (16)$$

and from here

$$q_{trans}^{(1)}(t) = \int_0^t (I_1(t) - I_{arc}(t))dt \quad (17)$$

Of course, $q_{trans}^{(1)}(t)/\Delta S_1$ is not exactly equal to $\rho_{trans}^{(1)}$. The charge does not distribute evenly on the patch. We can see this by static considerations:

$$\rho_{stat}^{(1)} = \beta\frac{q_{stat}^{(1)}}{\Delta S_1}. \quad (18)$$

The coefficient β denotes the ratio between a constant charge distribution and the real charge distribution. Now we assume that during the transient calculation the charge distribution on the lowest patch is similar to the static distribution:

$$\rho_{trans}^{(1)} = \beta \frac{q_{trans}^{(1)}}{\Delta S_1}. \tag{19}$$

$$E_{stat} + E_{trans}^{surf} = \frac{\beta}{\varepsilon_0 \Delta S_1}(q_{stat}^{(1)} + q_{trans}^{(1)}(t-(z-h)/c)). \tag{20}$$

The error introduced by this assumption decreases the smaller the current derivative and the larger the number patches are. After improving the simulation for the first patch we need to take a look at the voltage across the arc. From static consideration we can also see that E_{stat} integrated over the gap is not exactly the same as $2h \cdot E_{stat}(z=0)$. We introduce a second correction coefficient β_1:

$$\int_{-h}^{h} E_{stat}(z)dz = 2h \cdot \beta_1 \cdot \frac{\rho_{stat}}{\varepsilon_0}. \tag{21}$$

Again we assume that the static value of coefficient β_1 is suitable for the transient calculation. This allows expressing these coefficients by the static field integrated over the channel and the static charge.

Now we can write the arc equation as:

$$R(t)I_{arc}(t) + L\frac{dI_{arc}(t)}{dt} = \int_{-h}^{h} E_{stat}(z)dz \cdot \left(1 + \frac{q_{trans}^{(1)}}{q_{stat}^{(1)}}\right) \tag{22}$$

Using a simple numerical approximation for the time-derivative, we obtain an equation for the arc-current:

$$I_{arc}(t) = \frac{\int_{-h}^{h} E_{stat}(z)dz \cdot \left(1 + \frac{q_{trans}^{(1)}(t-\Delta t)}{q_{stat}^{(1)}}\right) + \frac{L}{\Delta t} I_{arc}(t-\Delta t)}{R(t) + \frac{L}{\Delta t}}. \tag{23}$$

Now lets consider the junction problem between the arc and the body.

The current in the lowest belt is denoted by $J^{(1)}(t)$. It is determined from the knowledge of the arc current by Kirchhoff's law. The second current density $J^{(2)}(t)$ and densities for all other belts are calculated by IEMF.

Even in the simpler linear case of a junction between a voluminous object and a perfectly conducting thin wire special care is needed [50,51,52]. Numerically this application is harder to handle for two reasons:

i) The arc is very short compared to the size of the body. Large charge and current density gradients exist close to the junction point.

ii) We need to calculate the electric field in the arc very accurately due to the extreme non-linearity of the ionization processes.

An space discretisation sufficiently fine enough to resolve these charges and currents would lead to unacceptably large run-times. Instead we divide the body into relatively large patches. Typically we use between 31 and 101 belts leading to a belt height of more than 6 mm which is large compared to the arc length of 0.1 ... 3 mm. As we do not take the real (and unknown) charge densities on each patch into account we introduce a relevant numerical error. Due to the highly nonlinear behavior of the arc we need to correct this error. This is done for the first two patches (nearest to the arc) by multiplying the fields radiated from them by a coefficients C_o and $2*(C_o-1)$ respectively. Using $C_0 = 1$ it is observed that the total charge flowing through the arc is not equal to the electrostatic charge stored at the beginning of the discharge. Now C_0 is slightly corrected until the total charge passing through the arc equals the electrostatic charge. Values for C_0 between 1.01 – 1.20 and tend to approach 1 the finer the discretization is chosen.

Let us summarize:

- The arc is modeled using the integral equation by Rompe and Weizel.
- Starting from literature data we improved Rompe and Weizel's coefficient a_R for ESD applications using an experiment which is independent from both the numerical calculation presented and the measurements used to validate the numerics.

The junction is treated using Kirchhoff's law and the electrodynamic solution is achieved using the magnetic integral equation, which is solved by MoM. To correct for errors caused by the discretization we introduce three correction factors. All of which are physically justified:

- β and β_1 are derived from the electrostatic field.
- C_0 and is derived from the total charge.

This leads to a complete numerical solution of the discharge process.

VI. NUMERICAL RESULTS

To validate the algorithm for perfectly conducting objects, we first compared the IEMF algorithm to literature data of linear scattering problems [47,48] and to analytical results for a spheroid [46]. Then we included the arc model and compared the calculated currents and fields with measured data of discharges from a spheroid with semi-axis 31 cm and 5 cm, a sphere and for a cone. A description of the measurement setup for current, fields and arc length can be found in [1].

In the Fig. 6 calculated and measured currents of the spheroid for different voltages and arc-lengths are compared.

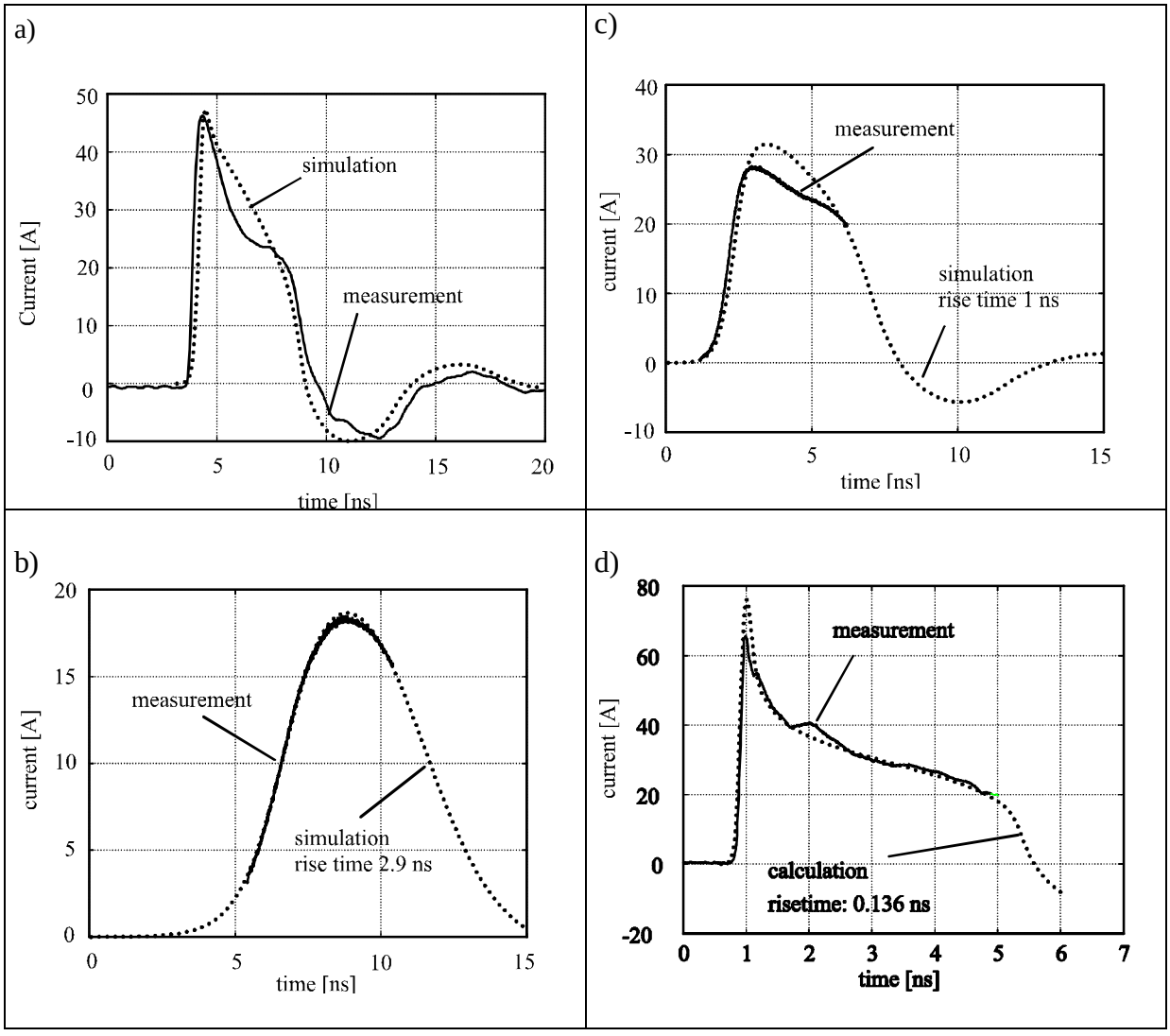

Fig.6. Comparison of calculated and measured arc-currents. Measurements used 5 kV independent of the distance to the ground plane.

a) h = 0.55 mm; $a_R = 1.8 \cdot 10^{-4}\ m^2/V^2s$; 1 GHz bandwidth

b) h = 1.116 mm; $a_R = 0.7 \cdot 10^{-4}\ m^2/V^2s$; 3.5 GHz bandwidth

c) h = 0.849 mm; $a_R = 1.38 \cdot 10^{-4}\ m^2/V^2s$; 3.5 GHz bandwidth

d) h = 0.323 mm; $a_R = 2.5 \cdot 10^{-4}\ m^2/V^2s$; 3.5 GHz bandwidth

The data of fig. 6 shows the ability to predict the current in spite of the large variation of current risetime. Although not strongly visible in the data shown one limitation of the arc model needs to be pointed out: As it neither takes recombination nor diffusion into account, the arc resistance can not increase again, i.e. one can not expect to be able to model current zero-crossings or current truncations. But from an EMC point of view this is not an important limitation as the initial current and field rise cause most of the disturbance threat by ESD.

Let us analyze ESD from the picture of the space-time distribution of currents on the spheroid (Fig.7).

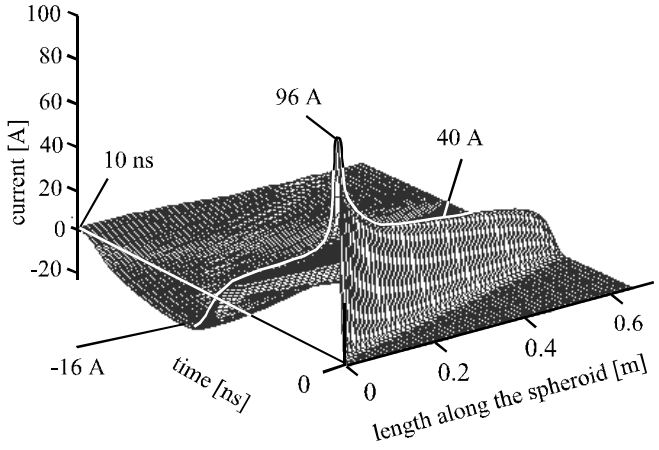

Fig. 7. Time-space distribution of the surface current on the spheroid at V = 5 kV, h = 0.314 mm, $a_R = 3.6 \cdot 10^{-4} m^2/V^2s$.

The initial current reaches 96 A. But only a 40 A current wave flows along the spheroid. The difference is caused by the charges, which had been close to the lower tip. They dominated the peak current, as shown in fig. 5. The current wave travels up to the top of the spheroid with little attenuation. At 2.1 ns the wave has reached the top of the spheroid where it gets reflected. In this moment the current changes direction and a strong electromagnetic field is radiated. The current wave propagates down to the channel. When it reaches the arc parts of it get reflected again.

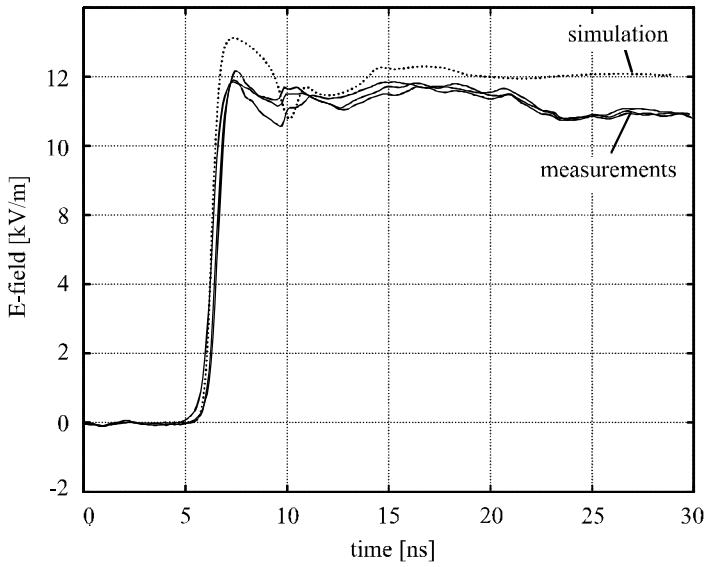

Fig. 8. Electric field of the spheroid on the ground plane at a distance of 0.3 m; V = 10 kV, h = 1.5 mm, $a_R = 2.1 \cdot 10^{-4}\ m^2 / V^2 s$

Knowing how a discharging body radiates into the space helps to define the required robustness and shielding of electronics in its vicinity. From the current distribution on the body the transient fields were calculated using integral expressions and compared to measurements as shown in figs.8 and 9.

The electric field shown in fig. 8 is displayed as a charging process; i.e. the static field is shown after the discharge, not prior to the discharge as it occurs in reality. This is due to the fact that the field sensors cannot measure DC-fields. Their lower cut-off frequency is at about 200 kHz. The sloping of the measured field data is also an effect of the lower cut-off frequency. For the magnetic field shown in fig. 9 larger differences occur after the zero crossing. This is probably due to the inability of the arc model to simulate current zero-crossings. Figs. 8 and 9 showed the fields on the ground plane. The spatial field distribution is shown in fig. 10. No free-space measurements were available to compare.

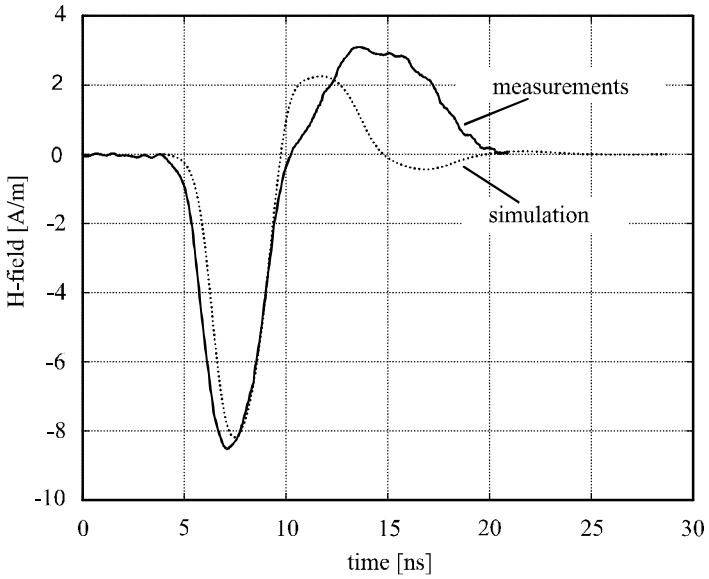

Fig 9. Magnetic field of the spheroid on the ground plane at a distance of 0.6 m; V = 10 kV, h = 2.0 mm, $a_R = 1.27 \cdot 10^{-4}\ m^2 / V^2 s$

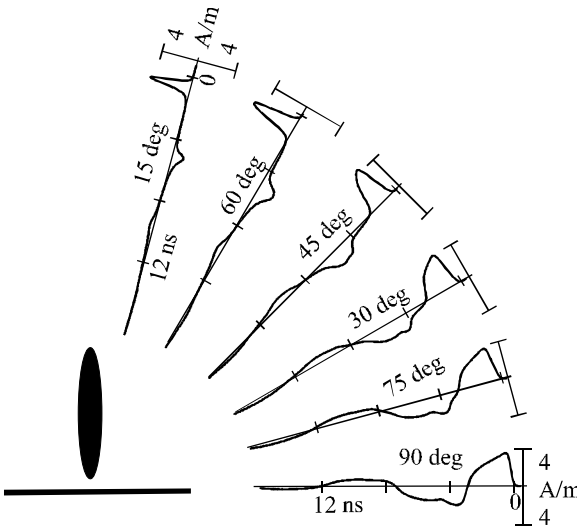

Fig.10. Magnetic field for different space directions at 1 m distance, V = 5 kV, h = 0.6 mm, $a_R = 2.51 \cdot 10^{-4}\ m^2 / V^2 s$.

Fig.11 shows the magnetic field for different directions in space at a distance of 1 m. The maximal values do not change much apart from very small angles. But the smaller the angle becomes the shorter the pulses get; i.e. fields contain higher frequency components.

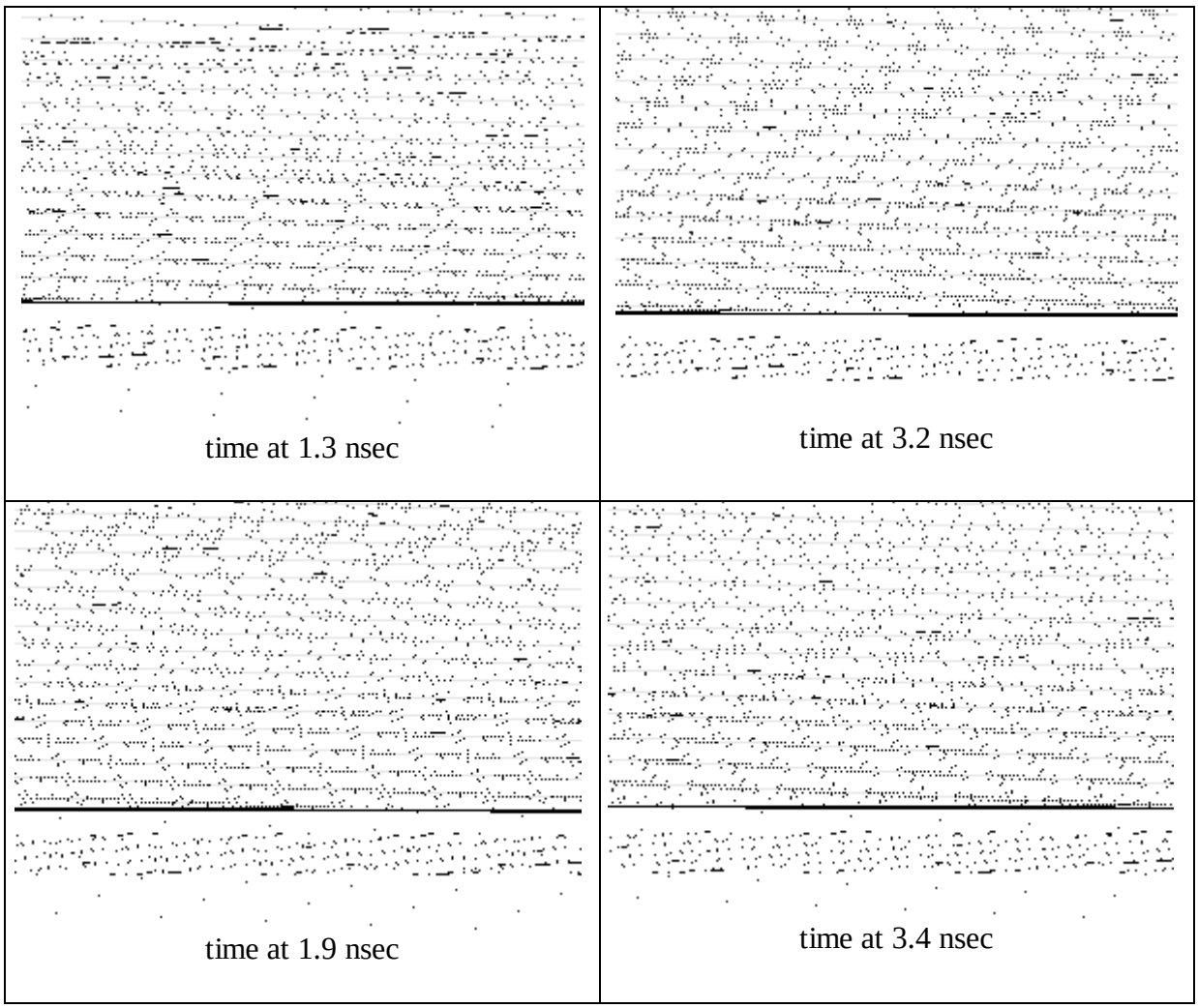

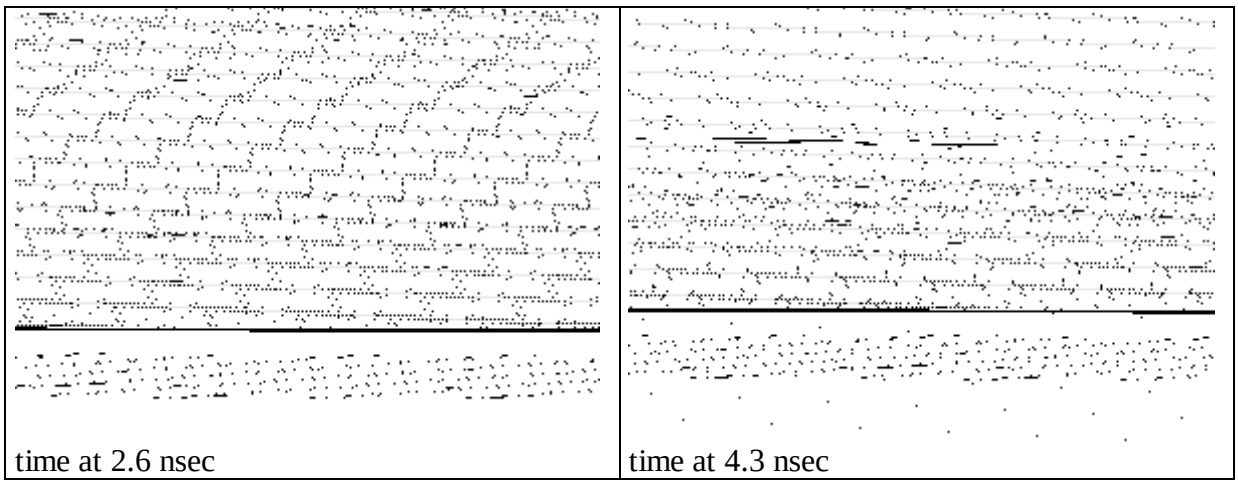

Fig. 11. Lines of constant magnetic field of the spheroid. V=10 kV. h=0.625 mm. $a_R = 3.5 \cdot 10^{-4}$

The time resolved process of radiation and wave guiding is shown in form of lines of constant magnetic field in Fig. 11. At 1.9 ns the initial current wave has traveled approximately 75% of the spheroid's length. At 3.2 ns the wave front has left the body. Although waves are radiated at every spot of the spheroid, the major radiation takes place at the upper and lower tips where the curvature is changing most rapidly. The last three pictures show that a large portion of the energy is guided by the surface and radiated in a direction of about 30^o for this very rapidly rising ESD event.

VII. COMPARISON TO TRANSIENT FIELDS FROM HUMANS

In most situations the first few nanoseconds of an ESD event determine the disturbance risk. Often it is sufficient to model this part of the event. With the exception of furniture ESD the most severe ESD event is the discharge of a human through a piece of metal. This is the reference for the widely applied ESD test standard IEC 61000-4-2. A spheroid of 0.2 and 0.02 m semi axis as shown in fig. 12 can approximate the hand/metal geometry.

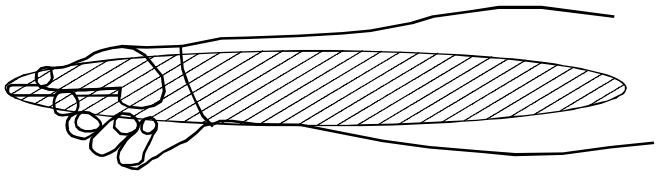

Fig.12. Hand/metal piece compared to a 0.2 m / 0.02 m spheroid.

This model allows simulating important parameters such as the peak values for current and fields and their derivatives, figs 13, 14 and 15. Other parameters, which are usually of lesser importance for EMC, like the total charge; the energy or the tailing current can not be modeled by this simplified geometry. But it is of great help to achieve a more realistic representation of the excitation in simulations, which solve coupling into circuits or enclosures [20]. It also allows analyzing the influence of humidity and speed of approach on ESD severity [53] as it includes the arc.

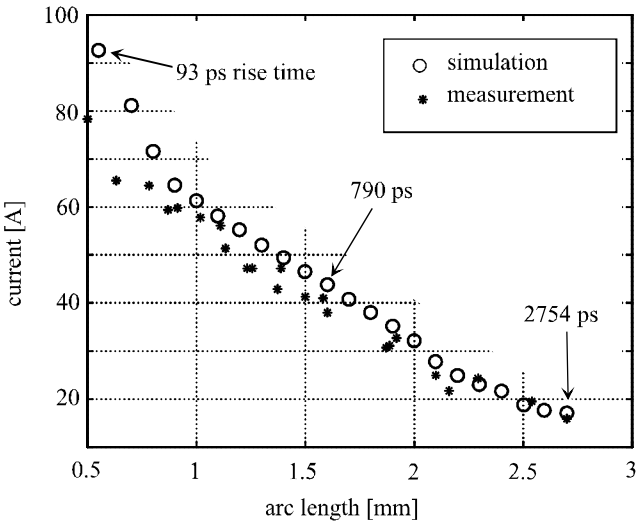

Fig.13: Peak current of a human/metal ESD (8 mm diameter, 75 mm long metal piece) at 10 kV compared to simulated ESDs of a 0.2 m, 0.02 m semiaxis spheroid. The value of a_R varied from 4 10^{-4} m^2/V^2s at 0.55 mm to 1 10^{-4} m^2/V^2s at 2.7 mm, see table 1. A Jon Barth Electronics current target was used which has a flat frequency response up to 10 GHz.

The simple model matches the measured peak current values shown in fig. 13 quite well. Discharges with an arc length of 2.7 mm (Paschen value) showed a rise time of 2.8 ns to 3.8 ns. For an arc length of 1.6 mm the current matches the simulator specifications given in IEC 61000-4-2 (rise time: 0.7-1 ns, peak value: 3.75 A/kV) at best: Its risetime is 0.79 ns and its peak value reaches 4 A/kV. For 5 kV the best match arc length is around 0.8 mm. Current derivatives are compared in fig.14.

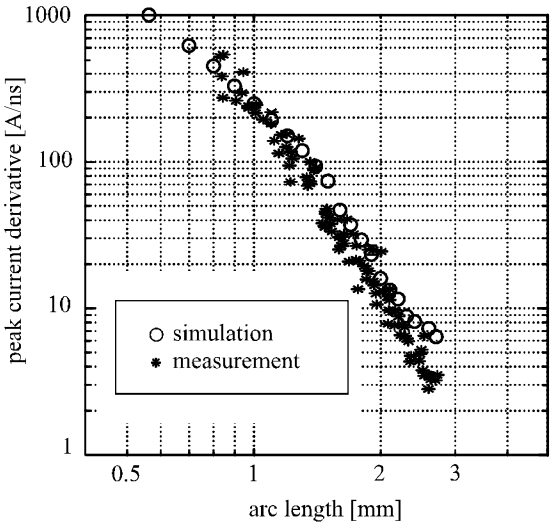

Fig14: Peak current derivative of a human metal ESD (6 mm diameter, 80 mm long metal piece) at 10 kV compared to simulated ESDs of a 0.2 m, 0.02 m semiaxis spheroid.

Simulated peak current derivatives vary from 6 A/ns to 1000 A/ns. They match the measured values well below 2 mm arc length. Above the measured derivatives are lower. As an example for the field the magnetic field at a distance of 0.5 m is shown in fig.15.

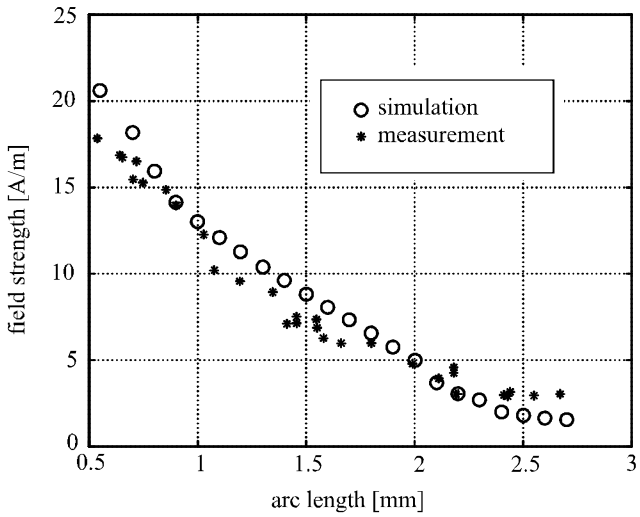

Fig15: Peak magnetic field of a human metal ESD compared to simulation using the same parameters as in fig. 15. The field was measured using a ground based B-dot sensor with self integration (2 MHz - 2 GHz +/- 1 dB) into an HP54720D oscilloscope (8 GS/s and 2 GHz analogue bandwidth) The distance was 0.5 m measured horizontally from the discharge point. The human stood in front of a vertical standing 2 m x 2 m ground plane.

The simulation matches the measured magnetic field quite well. Deviations at shorter arc lengths are a result of the 2 GHz measurement bandwidth limitation. For arc lengths above 2.5 mm the simulation provides lower values than the measurement. This is caused by not modeling the body discharge. In a human/metal ESD the longer the arc length is the smaller the initial current peak will be. But the discharge current of the body will not be influenced. Above some arc length the field radiated from the body current will be larger than the fields caused by the hand-metal structure. The transition at which both field components are of the same magnitude depend on the distance to the hand/metal structure and to the body. But attenuation on the arm and the charge accumulation at the tip of the metal piece will always cause a faster rising field from the hand/metal structure than from the body.

VIII. CONCLUSION

In this paper an ESD source model was presented. It combines a body of revolution with the non-linear arc and allows simulating parameters important for EMI of ESD such as peak currents, fields and their derivatives. Its strength lies in the inclusion of the extreme non-linear arc but its present implementation is limited to bodies of revolution.

Differences between measurements and simulations are less than +/- 20 % for the peak field and current values at most arc lengths and voltages and not more than +/- 50 % for extreme cases. The error must be judged against the strong influence of the arc length on the currents and fields. Peak field and current values vary by more than an order of magnitude with arc length for the same voltage and geometry. Peak derivative values vary by up to three orders of magnitude. Thus, the algorithm provides a good excitation model if coupling into circuits or enclosures is to be analyzed.

ACKNOWLEDGMENT

We want to thank the Volkswagen Foundation and the Deutsche Forschungsgemeinschaft for sponsoring this work.

APPENDIX

Glossary

Statistical time lag is the time interval in a high voltage breakdown which elapses between the moment at which the field strength reaches the value at which a breakdown is possible and the moment of the actual breakdown occurs. The delay is caused by the lag of seed electrons for the avalanche. Electrons attached to water molecules are the most important donors for seed electrons in practical ESD. Dry conditions cause long time lags [1,53].

Paschen value is the longest gap distance at which a breakdown is possible in a homogeneous electrostatic field. The value is calculated by Paschen's law [54].

Arc length is the gap distance in the moment of the breakdown. We assume straight arcs.

REFERENCES

[1] D. Pommerenke, "ESD: Transient Fields, Arc Simulation and Rise Time Limit," J. Electrostatics, vol.36, pp. 31-54, Oct. 1995.

[2] D. Pommerenke,'ESD: waveform calculation, field and current of human and simulator ESD', Journal of Electrostatics 38 (1996), 33-51

[3] A.Wallash, D.Smith, "Electromagnetic Interference (EMI) damage to giant magnetoresistive (GMR) recording heads", EOS/ESD Symp. 1998, pp 368-374

[4] D. Pommerenke, M. Aidam, "To What Extend do Contact Mode and Indirect ESD test Methods Reproduce Reality?" in Proc. EOS/ESD Symp., Phoenix, AZ, Sept., 12-14, 1995.

[5] B. Daout, H. Ryser, A. Germond, P. Zweiacker, "The Correlation of Rising Slope and Speed of Approach in ESD Tests", Int Zuerich Symp. on EMC 1987.

[6] P. Richman, "Progress Report on a Different Kind of ESD Standard", Int. Zurich Symp. on EMC 1989

[7] P.Richman, "Classification of ESD Hand/Metal Current Waves Versus Approach Speed, Voltage, Electrode Geometry and Humidity", Int. Zuerich Symp on EMC 1986.

[8] R.C.Pepe, "ESD Multiple Discharges", IEEE Int. Symp on EMC, 1991.

[9] D. Pommerenke, "Transiente Felder der ESD", Ph.D. dissertation, Technical University Berlin, VDI Forschrittberichte, Reihe 21 (Elektrotechnik), 1995.

[10] L. M. MacLeod, K. G. Balmain, "Compact Traveling Wave Physical Simulator for Human ESD" IEEE Trans. EMC, Vol. 39, No.2, May 1997

[11] W.T. Rhoades, "System ESD immunity design", Jour. of Electrostatics, 24(1990), pp.131-148.

[12] R.G. Reninger, "Mechanism of Charge Device ESD," EOS/ESD Symp. USA, 1991, p. 127-143.

[13] D.Pommerenke,"Sensoren zur Erfassung der transienten Felder der ESD", 107. Physikalisch-Technische-Bundesanstaldt, PTB Seminar. Thema: Feldsensoren, Dec. 1992

[14] P. F. Wilson, M. T. Ma, A. R. Ondrejka, "Fields radiated by electrostatic discharges", International Zurich Symposium on EMC 1988.

[15] S. Ishigami, T. Iwasaki, "Evaluation of charge transition in a small gap discharge", IEICE Trans. Commun, Vol.E79-B,no.4,pp.474-482.

[16] J.Ziman, K.Kovac, J.F.Dawson,"IEE Colloquim 'ESD (Electrostatic Discharge) and ESD Counter Measures'",Digest No. 1995/061, March 1995.

[17] S.Frei, D.Pommerenke, "Fields on the horizontal coupling plane excited by direct ESD and discharges to the vertical coupling plane", Jour. of Electrostatics 44 (1998), pp. 177-190

[18] O. Fujiwara, "An Analytical Approach to Model Indirect Effect caused by Electrostatic Discharges", IEICE Trans. on Commun, Vol. E79-B, No.4, pp. 483-489.

[19] M.Angeli, E.Cadelli,"Numerical Modeling of Electromagnetic Fields Generated by Electrostatic Discharges", IEEE Trans. on Magnetics, Vol.33, No.2, 1997, pp.2199-2202.

[20] S. van den Berghe, D. de Zutter,"Study of ESD signal entry through coaxial cable shields", Jour. of Electrostatics 44 (1998), pp. 135-148

[21] M.Rizvi, J.LoVetri,"ESD Source Modelling in FDTD", IEEE Int. Symp. on EMC 1994, pp.77-82

[22] B.S.Brown, L.L. Rauth,"Finite element time-domain simulation of electrostatic discharge using mixed-dimensional finite elements", IEEE Int. Symp. on EMC, 1994, pp.95-98

[23] O.Fujiwara, K.Kawaguchi, N.Kurachi, "FDTD Computation Modeling for Electromagnetic Fields Generated by Spark between Charged Metals", Int. Wroclaw Symp. on EMC, EMC'98, 1998

[24] M.Mardiguian,"Comments on 'Fields Radiated by Electrostatic Discharges' ", IEEE Trans on EMC, Vol.34, No.1, Feb. 1992

[25] M. Toepler, ”Zur Kenntnis der Gesetze der Gleitfunkenbildung,” Anmerkungen der Physik, 4. Folge, Band 21, 1906, pp. 193-222.

[26] M.Angeli, E.Cardelli, "Finite-Difference Frequency-Domain (FDFD) Modelling of EMI by ESD", IEEE Trans on Mag, Vol. 31, No.3, May 1995, pp.2064-2067

[27] G.Cerri, R.DeLeo, V.M.Primiani, M.Righetti, "Field Penetration into Metallic Enclosures Through Slots Excited by ESD", IEEE Trans. on EMC, Vol. 36, No.2, May 1994, pp. 110-116

[28] R. Zaridze, D. Karkashadze, G. Talakvadze, J. Khatiashvili, Z. Tzverikmazashvili, ”A Method of Auxiliary Sources in Applied Electrodynamics,” Proc. URSI Int. Symp. Electromagnetic Theory, Budapest, Hungary, Aug. 1986.

[29] D. Karkashadze, R. Zaridze, ”The Method of Auxiliary Sources in Applied Electrodynamics”, Latsis Symp. Computational Electromagnetics, Zurich, 1995, pp. 163-180.

[30] S.I Braginski, ”Theory of the Development of a Spark discharge:, Sov. Phys. JETP, 7 (1958) 1068-1074.

[31] R. Rompe, W. Weizel. ”Uber das Toeplersche Funkengesetz,” Z. Physik, Band 122, 1944, p. 636-639.

[32] G.A. Mesyats, ”Physics of Pulse Breakdown in Gases,” Moscow, Nauka Publisher, 1990, ISBN 5-02-014173-9, in Russian.

[33] G.A. Mesyats, G.S. Korshunov, "Formation of Nanosecond Sparks in Static Breakdown of a Gap", Sov. Phys. Tech. Phys. Vol. 13, No. 4, 1968, pp. 483-489.

[34] T.G. Engel, A.L. Donaldson, M. Krisiansen. "The Pulsed Discharge Arc Resistance and its Functional Behavior", 1989 IEEE Trans. on Plasma Science, Vol. 17, No. 2.

[35] H.M. Hyatt, ”The resistive Phase of an Air Discharge and the Formation of Fast Rise Time ESD Pulses.” EOS/ESD Symp. 1992.

[36] Gruenberg, "Gesetzmaessigkeiten von Funkenentladngen im Nanosekundenbereich", Z. Naturforschung A, 20a, 1965, pp. 202-212.

[37] V.M. Ristic, G.R. Dubois, :Time Dependent Spark-gap Resistance in Short Duration Arcs with Semimetallic Cathods,” IEEE Trans. Plasma Sci., PS-6 (4) 1978.

[38] V.M. Ristic, G.R. Dubois, :Time Dependent Spark-gap Resistance in Short Duration Arcs with Semimetallic Cathods,” IEEE Trans. Plasma Sci., PS-6 (4) 1978.

[39] H.M. Hyatt, ”The resistive Phase of an Air Discharge and the Formation of Fast Rise Time ESD Pulses.” EOS/ESD Symp. 1992.

[40] G.A. Mesyats, V.V. Kremnev, G.S. Korshunov, Yu. B. Yankelevich, "Spark Current and Voltage in Nanosecond Breakdown of a Gas Gap", Sov. Phys. Tech. Phys. Vol. 14, No. 1, 1969, pp. 49-53.

[41] R.E.Carey, L.F.DeChiaro, "An experimental and theoretical consideration of physical design parameters in field-induced charged device model ESD simulators and their impact upon measured withstand voltages", EOS/ESD Symp. 1998, pp.40-53

[42] C.L. Bennett, ”Time-domain Solution of Transient Problems”, in Lectures on Computational Methods in Electromagnetics. (Eds: Harrington R.F., Wilton D.R., Buttler C.M., Mittra R., Bennett C.L.) St. Cloud, ACEEE Press, 1981.

[43] A.J. Poggio, E.K. Miller, ”Integral Equation Solutions of Tree-dimensional Scattering Problems”, in Computer Techniques for Electromagnetics, Oxford Pergamon Press, 1973, pp. 159-264.

[44] H. Mieras, C.L. Bennett, ”Space-time Integral Approach to Dielectric Targets”, IEEE Trans. Antennas Propagat., Vol. AP-30, pp. 2-9, 1982.

[45] R. Mittra, ”Integral Equation Methods for Transient Scattering” in Transient Electromagnetic Fields, Ed. L.B. Felsen, Berlin, Springer Verlag, 1976, pp. 73-126.

[46] J. Mautz, R. Harrington, ”Radiation and Scattering from Bodies of Revolution”, Appl. Sci. Res. June 20, 1969, pp. 405-434.

[47] R. Jobava, P. Shubitidze, R. Zaridze, D. Karkashadze. ”Investigation of the Transient Electromagnetic Field Radiated or Scattered by Three-Dimensional Conducting Bodies”. Proc. of VI-th Int. Conf. in Mathematical Methods in Electromagnetic Theory (MMET’96) Sept. 10-13, 1996, Lviv, Ukraine, pp. 323-327.

[48] P. Shubitidze, R. Jobava, D. Karkashadze, D. Pommerenke, R. Zaridze. ”Electrostatic Discharge of Objects with Surface Resistance”. Bulletin of the Georgian Academy of Sciences. Vol. 155, 12, 1997, pp. 185-191.

[49] R. Zaridze, D. Karkashadze, R. Djobava, D. Pommerenke, M. Aidam. ”Numerical Calculation and Measurement of Transient Fields from Electrostatic Discharge” IEEE Trans. on Components, packaging, and manufacturing Technology, Part C: Manufacturing, v.19, July 1996, No. 3, pp. 178-183.

[50] E.H. Newman, D.M. Pozar, "Electromagnetic modeling of composite wire and surface geometries," IEEE AP-26, No.6, 784-788, 1978.

[51] L.N. Medgiesi-Mitschang, J.M. Putnam, "Formulation for wire radiators on bodies of translation with and without end caps," IEEE AP-31, No.6, 853, 1983.

[52] S. Bhattacharia, S.A. Long, D.R. Wilton, "The input impedance of a monopole antenna mounted on a cubical conducting box," IEEE AP-35, 756-762, 1987.

[53] S.Frei, M.Senghaas, R.Jobava, W.Kalkner, "The influence of speed of approach and humidity on the intensity of ESD", Int. Zuerich Symp. on EMC 1998

[54] Meek and Crags, Electrical Breakdown of Gases, Oxford univ. Press, Oxford, 1953 and Wiley, New York, 1978.